JOURNAL OF AIRCRAFT
Vol. 46, No. 5, September–October 2009

Identification of a Nonlinear Wing Structure Using an Extended Modal Model

M. F. Platten*
Romax Technology, Nottingham, England NG7 2PZ, United Kingdom
J. R. Wright†
University of Manchester, Manchester, England M60 1QD, United Kingdom
J. E. Cooper‡
University of Liverpool, Liverpool, England L69 7ZE, United Kingdom
and
G. Dimitriadis§
University of Liège, 4000 Liège, Belgium

DOI: 10.2514/1.42024

The nonlinear resonant decay method identifies a nonlinear dynamic system using a model based in linear modal space comprising the underlying linear system and a small number of additional terms that represent the nonlinear behavior. In this work, the method is applied to an aircraftlike wing/store/pylon experimental structure that consists of a rectangular wing with two stores suspended beneath it by means of nonlinear pylons with a nominally hardening characteristic in the store rotation degree of freedom. The nonlinear resonant decay method is applied to the system using multishaker excitation. The resulting identified mathematical model features five modes, two of which are strongly nonlinear, one is mildly nonlinear, and two are completely linear. The restoring force surfaces obtained from the mathematical model are in close agreement with those measured from the system. This experimental application of the nonlinear resonant decay method indicates that the method could be suitable for the identification of nonlinear models of aircraft in ground vibration testing.

I. Introduction

THE identification of nonlinear dynamic systems is a topic of considerable current interest, given that many real systems exhibit nonlinear characteristics [1]. Methods range from those that allow detection of the presence of nonlinear effects, through indicating the classification of the type of nonlinearity present, to methods that seek to identify a mathematical model for the nonlinear system under test. The latter class of methods is of most interest, as they allow the response of the system to be predicted and they potentially enable structural modification studies or other interventions to be carried out.

It is generally accepted that recent developments in aerospace engineering, such as active control systems and increasingly flexible structures, have rendered aircraft more nonlinear. Furthermore, traditional sources of nonlinearity such as backlash in bearings and store pylons are still present. Therefore, the true vibrational characteristics of an aircraft can only be obtained if the nonlinearity present in the structure and control system is quantified and identified.

Because of these considerations, there is increasing interest in ground vibration tests (GVTs) for aircraft that can detect, characterize, and identify nonlinearity. Current GVT methodologies can only readily detect nonlinearity using stepped sine or phase resonance [2] tests. Several extensions to this methodology have been proposed, such as the nonlinear resonant decay method (NL-RDM) [3,4], phase-separation techniques [2,5], nonlinearity detection by wavelet transforms of impulse responses [6], describing functions [7] (also called linearity plots [8] or modal characterizing functions [9]), identification of nonlinearities by time-series-based linearity (INTL) plots [10], neural networks [11], expert systems [12], and Hilbert transforms [9].

Nonlinear system identification can be performed in physical space (i.e., using measured inputs and responses for parameter estimation) or in modal space (using modal responses). Aircraft-specific work usually focuses on modal models due to the high level of complexity of aircraft structures [3–5,8,10]. The usual assumption is that aircraft are mostly linear dynamic systems that contain some weakly nonlinear modes. These modes behave nearly linearly under small amplitudes of excitation. Consequently, a linear modal model is a good approximation of the true aircraft at low excitation levels and a good basis for a nonlinear model.

The focus in this paper is on a particular approach to identifying a nonlinear aircraft model based in linear modal space. The NL-RDM was first proposed in 2001 [3] and further detailed in subsequent publications [4,13]. It aims to identify a model based in linear modal space, the so-called extended modal model. It is fundamentally based upon a development of the original restoring force surface approach in modal space [14] and takes advantage of the methodologies for normal mode force appropriation [15]. In fact, the NL-RDM was the first approach to propose the application of appropriated excitation to nonlinear systems to limit the number of responding modes [3]. It seeks to consider modes as being in one of several categories: namely, 1) modes that behave linearly, 2) modes that behave nonlinearly but are not nonlinearly coupled to other modes, and 3) modes that are nonlinear and are nonlinearly coupled to other modes. Each of the modes behaving nonlinearly (i.e., categories 2 and 3) may then be identified using a relatively-low-order model in which a limited number of nonlinear modal terms (usually, but not necessarily, of polynomial type) extend the linear modal equation for that mode to account for the nonlinear effects. The use of appropriated force patterns provides a coarse filter in which each mode of interest is

Received 5 November 2008; revision received 2 June 2009; accepted for publication 11 June 2009.

*Research Engineer, Noise, Vibration and Harshness Team, Rutherford House, Nottingham Science and Technology Park; michaelp@romaxtech.com.

†Professor, School of Mechanical, Aerospace and Civil Engineering, P.O. Box 88; jan.wright@manchester.ac.uk

‡Professor, Department of Engineering, Chadwick Tower, Peach Street; j.e.cooper@liverpool.ac.uk. Member AIAA.

§Assistant Professor, Aerospace and Mechanical Engineering Department, Chemin des Chevreuils 1; gdimitriadis@ulg.ac.be. Member AIAA.

driven more strongly than others, thus reducing the complexity of the identification required.

As mentioned previously, other system identification strategies based on a model in modal space and the restoring force surface method have been presented: in 2004, Göge et al. [10,16] proposed the INTL approach. Modes that are known to behave nonlinearly are appropriated. The sinusoidal generalized force and modal acceleration responses are used to calculate the nonlinear restoring force. The nonlinear stiffness and damping terms are curve-fitted separately using polynomial or other basis functions. Then a harmonic balance expansion is performed on the fitted restoring force surface to obtain linearity plots (plots of frequency and damping dependence on excitation amplitude). In 2007, Göge [9] introduced additional steps for quickly determining the modes that behave nonlinearly. All the INTL-based approaches use either sinusoidal or very-narrowband chirp excitations and responses to perform the nonlinear curve fit. It should be stressed that INTL-based approaches do not consider nonlinear (or linear for that matter) cross-coupling terms. Göge et al. [10] stated that a perfect appropriation of nonlinear modes is possible, so that only the nonlinear mode of interest will respond. They justified this statement by referring to the force appropriation by nonlinear systems (FANS) approach proposed by Atkins et al. [17], although they did not actually use this technique.

The NL-RDM method differs from the INTL-based approaches in that it allows for nonlinear cross coupling. The FANS approach [17] makes use of an optimization procedure to perfectly appropriate nonlinear modes. This optimization procedure is very time-consuming and not ideally suited to aircraft ground vibration tests. Classical (nonoptimized) force appropriation significantly reduces the response of nonlinearly cross-coupled modes but does not eradicate it. Therefore, any nonlinear mathematical model used for the identification of nonlinear aircraft structures must allow for nonlinearly coupled modes.

Furthermore, the NL-RDM uses responses resulting from burst excitation in the nonlinear curve-fitting. The method involves exciting the structure with a burst sine or narrowband chirp at the natural frequency of the mode of interest; after the end of the burst excitation, the responses are allowed to decay freely. The complete force and response signals are used to perform the nonlinear identification of the mode. As only the appropriated mode and the modes that are nonlinearly coupled to it respond, the identified nonlinear model is of low complexity and the number of candidate terms is low.

The NL-RDM has been applied successfully to a number of simulated systems [3,4] up to 9 degrees of freedom and also experimentally to a clamped panel structure [4,13], in which a nonlinear description of the first three modes, all behaving nonlinearly due to stretching of the plate's middle surface, was obtained. The structure was continuous and the nonlinearity was distributed. Note that a linear model could be used to represent higher-frequency modes in which nonlinear effects are negligible.

In this paper, a more complex experimental model is constructed to represent a wing with two stores suspended under the wing via pylons. Each store/pylon is able to rotate about a nonlinear hardening spring arrangement just below the wing. As such, the model is representative of a continuous aircraft structure with discrete nonlinear elements, featuring close modes and nonlinear coupling. The NL-RDM approach is applied to this system to determine how well the method is able to identify such a structure over the frequency range encompassing the first five flexible modes.

II. Nonlinear Resonant Decay Method

The theoretical basis of this method has been detailed elsewhere [4] but will be outlined here for completeness. To allow continuous multi-degree-of-freedom nonlinear systems to be identified, the identification process takes place in linear modal space. If the modal matrix of the underlying linear system may be identified, then it is possible to transform measured responses and forces from physical to modal space.

The equations of motion of an aircraft can be written to include nonlinear terms such that

$$\bar{\mathbf{M}}\,\ddot{\mathbf{w}} + \bar{\mathbf{C}}\,\dot{\mathbf{w}} + \bar{\mathbf{K}}\mathbf{w} + \mathbf{f}_{\mathrm{NL}}(\mathbf{w}, \dot{\mathbf{w}}) = \bar{\mathbf{f}}(t) \tag{1}$$

where $\bar{\mathbf{M}}$ is a $N \times N$ mass matrix, $\bar{\mathbf{C}}$ is a $N \times N$ linear damping matrix, $\bar{\mathbf{K}}$ is a $N \times N$ linear stiffness matrix, $\mathbf{f}_{\mathrm{NL}}$ is a $N \times 1$ vector of nonlinear functions, $\mathbf{f}(t)$ is a $N \times 1$ vector of excitation forces, $\mathbf{w}$ is a $N \times 1$ vector of physical displacements, and N is the number of physical coordinates. Such a set of equations can be obtained, for example, from the finite element modeling of an aircraft.

It is assumed that a modal representation of the system can be achieved through the transformation

$$\mathbf{w} = \mathbf{\Phi}\mathbf{p} \tag{2}$$

where $\mathbf{p}$ is a $N_R \times 1$ vector of modal displacements, N_R is the number of retained modes and $\mathbf{\Phi}$ is a $N \times N_R$ modal transformation matrix. For a general nonlinear system, such a transformation would be meaningless. However, it is assumed that an aircraft can be idealized as a system that is mainly linear and features a small number of nonlinear modes, which behave clearly in a nonlinear manner only when excited to a high energy level. Under this assumption, the transformation of Eq. (2) leads to the modal representation of the underlying linear system: that is, a linear system that behaves in a manner almost identical to that of the full nonlinear system under low-amplitude excitation.

The equations of motion of the underlying linear system in modal space are given by

$$\mathbf{M}\,\ddot{\mathbf{p}} + \mathbf{C}\dot{\mathbf{p}} + \mathbf{K}\mathbf{p} = \mathbf{f}(t) \tag{3}$$

where $\mathbf{M} = \mathbf{\Phi}^T\bar{\mathbf{M}}\mathbf{\Phi}$, $\mathbf{C} = \mathbf{\Phi}^T\bar{\mathbf{C}}\mathbf{\Phi}$, $\mathbf{K} = \mathbf{\Phi}^T\bar{\mathbf{K}}\mathbf{\Phi}$, and $\mathbf{f} = \mathbf{\Phi}^T\bar{\mathbf{f}}$. If the aircraft structure features proportional damping, then it is well known that its equations of motion in linear modal space are in nominally single-degree-of-freedom form: namely,

$$m_r\ddot{p}_r + c_r\dot{p}_r + k_r p_r + f_{\mathrm{NL}_r} = f_r(t) \tag{4}$$

for $r = 1, 2, \ldots, N_R$, where p_r is the rth modal displacement; m_r, c_r, and k_r are the rth-mode modal mass, damping and stiffness; and f_r is the applied modal force. The modal mass and stiffness for the linear system are related by the undamped natural frequency. Nonproportional damping would lead to the presence of modal damping coupling terms. The term f_{NL_r} refers to the rth-mode nonlinear modal restoring force and, in general, includes modal coordinates from other modes to allow for nonlinear cross-coupling terms. A typical polynomial expression for this nonlinear restoring force, involving the rth and jth modal displacements and including nonlinear terms up to cubic in order, might be

$$f_{\mathrm{NL}_r} = A_1 p_r^2 + A_2 p_r p_j + A_3 p_j^2 + A_4 p_r^3 + A_5 p_r^2 p_j + A_6 p_r p_j^2 + A_7 p_j^3 \tag{5}$$

This expression includes only nonlinear stiffness terms, as witnessed by its dependence on modal displacements only. Nonlinear damping, such as quadratic damping, can be modeled by including terms depending on modal velocities; for example,

$$f_{\mathrm{NL}_r} = A_1 p_r^2 + A_2 p_r p_j + A_3 p_j^2 + A_4 p_r^3 + A_5 p_r^2 p_j + A_6 p_r p_j^2 + A_7 p_j^3 + A_8\dot{p}_r|\dot{p}_r| + A_9\dot{p}_r|\dot{p}_j| + A_{10}\dot{p}_j|\dot{p}_r| + A_{11}\dot{p}_j|\dot{p}_j| \tag{6}$$

Other nonlinearities can be modeled using suitable basis functions. Göge et al. [8] provided an extended list of nonlinearities and the functions that can be used to model them.

The definition of f_{NL_r} is the crucial difference between the NL-RDM and INTL-based approaches [9,10]. The NL-RDM allows for contributions from other modes in f_{NL_r}, and INTL-based approaches only allow direct contributions (i.e., only terms involving p_r). As

already mentioned, cross-coupling terms must be included for a good-quality identification, because the force appropriation of each mode cannot be perfect.

The idea of the NL-RDM is that the natural frequency, damping ratio, mode shape, modal mass, and hence linear modal stiffness for each mode may be identified using classical methods, based on data extracted at relatively low levels of excitation for nonlinearities for which the influence grows with increasing amplitude. For nonlinearities such as free play, more important at low amplitude, an underlying linear model may be extracted by exciting the system at relatively high amplitudes [18]. In addition, the appropriated force vectors required to excite each normal mode of the system may be estimated using the multivariate mode indicator function (MMIF) method [14].

Any mode that behaves linearly [seen, for example, by comparing frequency response functions (FRFs) at several excitation levels] is then fully defined by its modal parameters and no further nonlinear identification step is necessary. However, any mode that behaves nonlinearly, either because there are direct modal nonlinear terms in the modal equation or because it is coupled nonlinearly to other modes, will need to be identified further.

The NL-RDM normally involves exciting a mode of interest using a burst of sine excitation at the undamped natural frequency of the mode and using the appropriated force vector determined from the MMIF [15] method; the appropriated excitation is aimed at exciting a dominant response in the mode of interest to minimize the number of other modes involved in the identification process. The measured accelerations and forces are converted into modal space and the accelerations are integrated to estimate modal velocities and displacements; the burst nature of the excitation and response is such that the double integration may be performed in the frequency domain with minimal leakage errors.

Burst excitation refers to the case in which the excitation is only applied during a fraction of the total force and response measurement time. Assuming that force and response signals are measured from time 0 to time t_f, a burst excitation starts at time instance t_1 and finishes at time instance t_2, where $0 < t_1 < t_2 < t_f$. Three types of burst are considered for application with the NL-RDM method: square, triangular, and $1 - \cos$.

A square burst sine is given by the equation

$$f_r(t) = \begin{cases} 0 & \text{for } t < t_1 \\ A_0 \sin \omega_r t & \text{for } t_1 < t < t_2 \\ 0 & \text{for } t_2 < t < t_f \end{cases} \tag{7}$$

where A_0 is the desired amplitude of excitation and ω_r is the undamped natural frequency of the rth mode of the underlying linear system, given by $\omega_r = \sqrt{k_r/m_r}$.

A triangular burst sine is given by the equation

$$f_r(t) = \begin{cases} \frac{A_0}{t_1} t \sin \omega_r t & \text{for } t < t_1 \\ A_0 \sin \omega_r t & \text{for } t_1 < t < t_2 \\ A_0 \left(1 - \frac{t - t_2}{t_f - t_2}\right) \sin \omega_r t & \text{for } t_2 < t < t_f \end{cases} \tag{8}$$

That is, the amplitude of the signal increases linearly with time until the desired amplitude is achieved. It also decreases linearly with time after time t_2. Finally, the $1 - \cos$ burst sine is given by the equation

$$f_r(t) = \begin{cases} \frac{A_0}{2} \left(1 - \cos \frac{\pi}{t_1} t\right) \sin \omega_r t & \text{for } t < t_1 \\ A_0 \sin \omega_r t & \text{for } t_1 < t < t_2 \\ \frac{A_0}{2} \left(1 + \cos \frac{\pi}{t_f - t_2} (t - t_2)\right) \sin \omega_r t & \text{for } t_2 < t < t_f \end{cases} \tag{9}$$

That is, the amplitude of the signal increases with time in a $1 - \cos$ manner until the desired amplitude is achieved. It decreases in a $1 + \cos$ manner after time t_2. Figure 1 shows examples of all three types of burst sine signals. The triangular and $1 - \cos$ burst sine signals are used to avoid the impulsive responses that can be caused by the abrupt jump in the amplitude of the square burst signal. In systems with very low damping, these impulsive responses can be quite pronounced, can excite all modes, and can degrade the quality of the subsequent curve fit. They therefore defeat the purpose of appropriated excitation.

After the application of the excitation and the measurement of the force and response signals, sufficient information is available to estimate the rth-mode nonlinear modal restoring force f_{NL_r}, as a function of time, using the equation

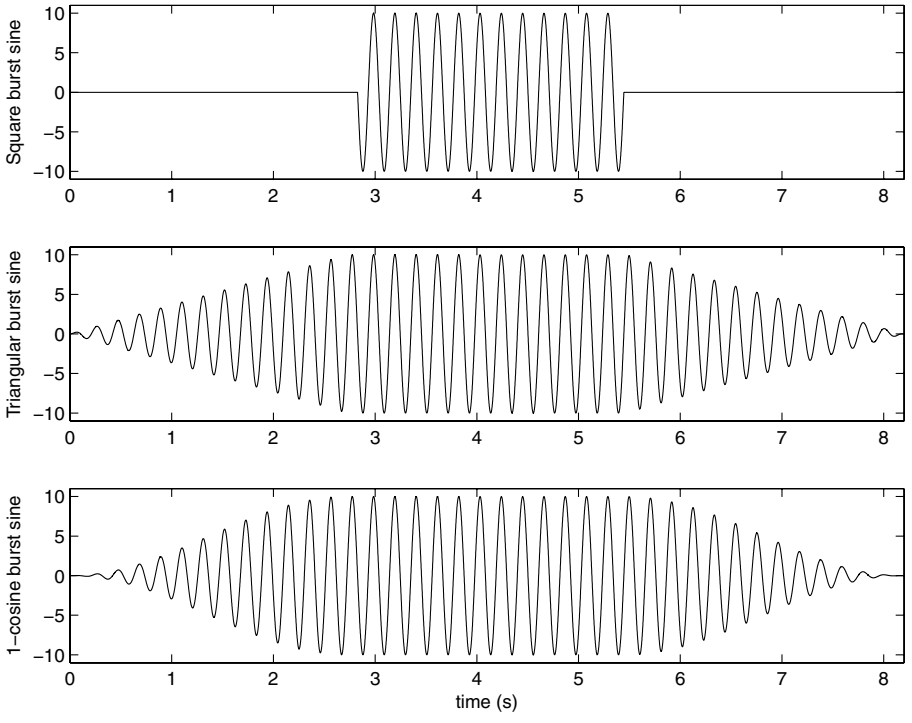

Fig. 1 Three types of burst sine excitation: square (top), triangular (middle), and $1 - \cos$ (bottom).

$$f_{\mathrm{NL}_r} = f_r(t) - m_r\ddot{p}_r - c_r\dot{p}_r - k_r p_r \tag{10}$$

for $r = 1, 2, \ldots, N_R$. Using a suitable polynomial (or other) representation for the restoring force, such as Eq. (6), a curve fit may be performed to estimate the polynomial coefficients, with coupling terms to other modes included if necessary. This approach is effectively a direct parameter estimation procedure, as described by Worden and Tomlinson [1]. The model order is adjusted to achieve a suitable goodness of fit. The process is repeated for all modes that behave nonlinearly and the results are then combined with the linear modes to create a full set of modal equations, some linear and others nonlinear. The system response may then be estimated for any specified forcing input.

To summarize, the characteristics of the NL-RDM approach are the following:

1) Only one equation of motion is normally curve-fitted at a time. Nonlinear system identification generally works best when single-degree-of-freedom systems are identified.

2) Force appropriation aims to ensure that only the mode of interest and all the modes nonlinearly coupled to it respond. Therefore, the number of responses used in the curve fit, and hence the number of candidate terms, is low.

3) By applying a burst excitation and then observing the decaying responses, the complete nonlinear restoring force is visualized. Therefore, a better assessment of the most suitable basis functions to use in the curve fit can be made.

4) The burst nature of the response signals allows the accurate numerical integration of acceleration measurements to obtain high-quality velocity and displacement estimates.

III. Wing/Pylon/Store Experimental Model

The continuous test structure used in this paper is intended to represent approximately the configuration of an aircraft wing having two underwing stores (e.g., engines, fuel tanks, etc.), with nonlinear pylon connections between them. The fact that underwing stores can introduce nonlinearities has been known since Breitbach [19]. More recently, Beran et al. [20] reported that the presence of an attached store/pylon introduces nonlinear kinematical terms in the equations of motion of a cantilever wing. Additionally, Göge et al. [8] showed GVT results demonstrating that underwing engines mounted on pylons can exhibit free play in the yaw mode.

The wing created for the present experiments consists of a rectangular aluminum plate supported using bungee chords and two stores suspended beneath the wing via pylons, as shown in Fig. 2. The nonlinear pylon/store support arrangement was based on clamping the pylon plates in a variable-profile clamp, as shown in Fig. 3. In this clamp, the pylon plates become shorter, and therefore stiffer, as they are deflected laterally. The exact clamp profile was calculated numerically, with the objective being to generate a near-cubic hardening stiffness arrangement. The clamp surfaces were machined numerically.

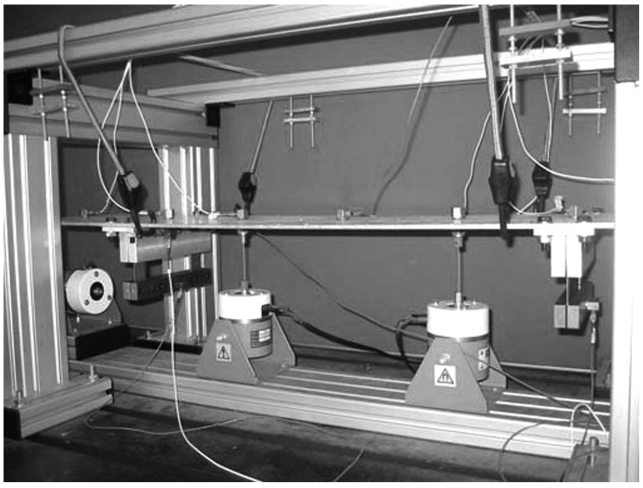

Fig. 2 Photograph of wing/pylon/store arrangement.

IV. Experimental Arrangement

Figure 2 also shows the arrangement of the model, supported from a frame via bungee chords in a nominally free–free configuration. The bungees should ideally have been longer to reduce the rigid-body frequencies, which were around 20% of the first flexible mode. Two Gearing and Watson V4 shakers were attached to the centerline of the wing via force gauges and driven by Gearing and Watson power amplifiers using a constant current; the aim was to excite and measure bending and not torsion modes. It was found previously that when the shakers were attached to the store masses, the allowable armature motion was insufficient to allow the required motion for the pylon arrangement under investigation to behave sufficiently nonlinearly. In total, nine accelerometers were positioned along the centerline of the wing and on the two stores, as shown in Fig. 4. Acceleration and force were measured using PCB Piezotronics transducers. An LMS SCADAS III data acquisition system was employed for excitation and measurement of the model, using various advanced test and analysis software packages, as well as user-developed programs.

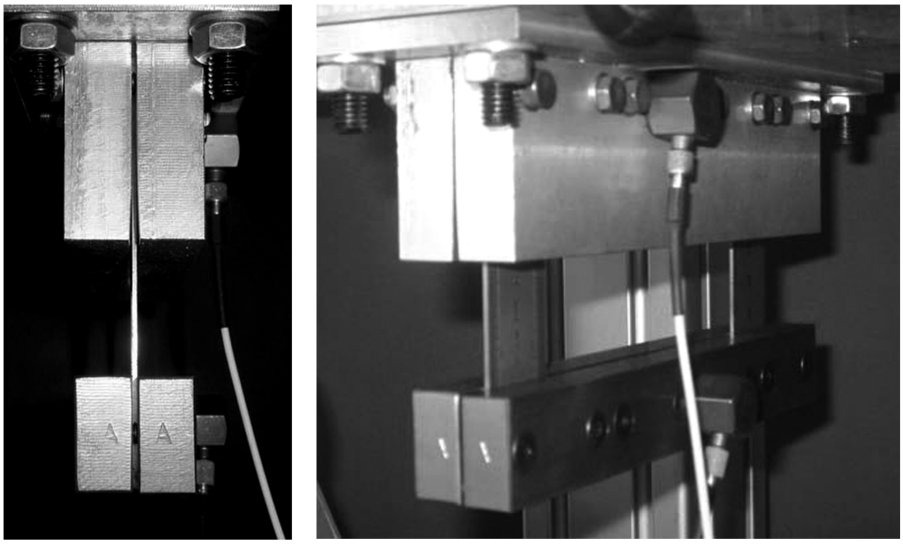

a) Front view **b) Side view**

Fig. 3 Variable-profile clamp arrangement.

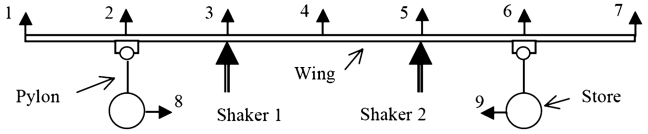

Fig. 4 Diagram of wing/pylon/store arrangement with accelerometer and shaker positions.

V. Static and Dynamic Characteristics of Store/Pylon

A. Static Characteristics of Store/Pylon Arrangement

Because each store/pylon arrangement could be detached from the wing, it was decided to first perform a static load test on the two assemblies. Load/deflection curves for both store/pylons are shown in Fig. 5, and it is clear at first sight that a hardening stiffness characteristic is present. The curve for each store/pylon was fitted using a cubic polynomial; the resulting equations were

$$L_1 = 3.28 \times 10^8 x_1^3 + 3.39 \times 10^5 x_1^2 + 7.70 \times 10^3 x_1 - 0.01 \quad (11)$$

$$L_2 = 3.65 \times 10^8 x_2^3 + 4.87 \times 10^5 x_2^2 + 7.39 \times 10^3 x_2 + 0.48 \quad (12)$$

where L_1 is the load on store 1, L_2 is the load on store 2, x_1 is the deflection of load 1, and x_2 is the deflection of store 2. It is clear that both assemblies feature a slight asymmetry, as the polynomial curve fits contain constant and second-order terms. Additionally, there was some difference between the stiffness values of the two store/pylons, as it was not possible to construct both identically. The cubic and square term coefficients also differ between stores; consequently, in the ±65 N load range, store assembly 2 (Fig. 5b) is slightly more nonlinear than store assembly 1 (Fig. 5a).

B. Dynamic Characteristics of Store/Pylon Arrangement

To further explore the store/pylon assembly characteristics, it was decided to undertake a dynamic test. A hammer test was carried out on the unit to generate a freely decaying response. The decaying time history of Fig. 6 shows a classical single-degree-of-freedom form, with no obvious nonlinear effects. The presence of a stiffness nonlinearity would be seen by a variation in natural frequency with amplitude and of a damping nonlinearity by changes in damping ratio with amplitude. It is possible that there is a very slight nonlinear damping effect, seen by studying the logarithm of the decay, as seen in Fig. 6b; for a linearly damped system, the envelope of the logarithm of the decay should be a straight line.

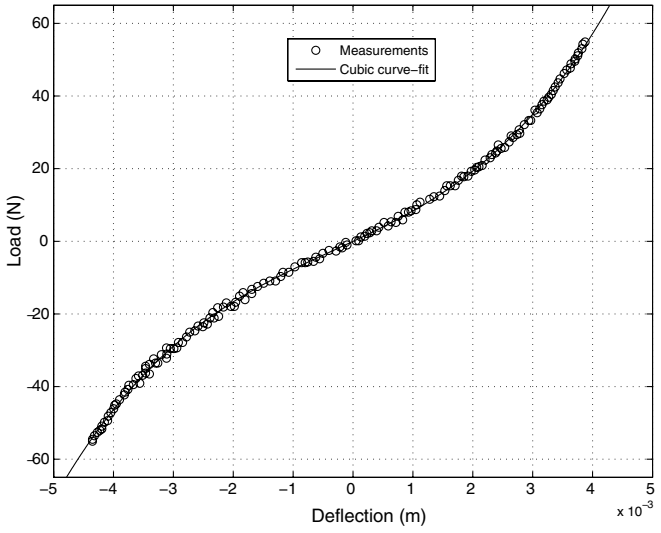

a) Store 1

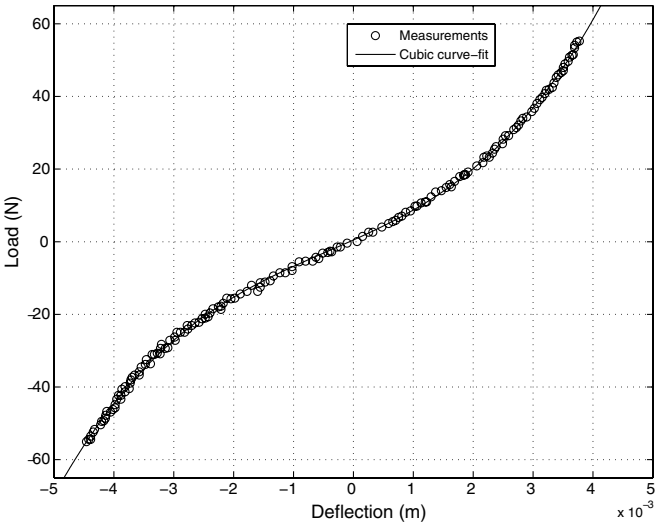

b) Store 2

Fig. 5 Static load/deflection curves for the two store/pylon assemblies.

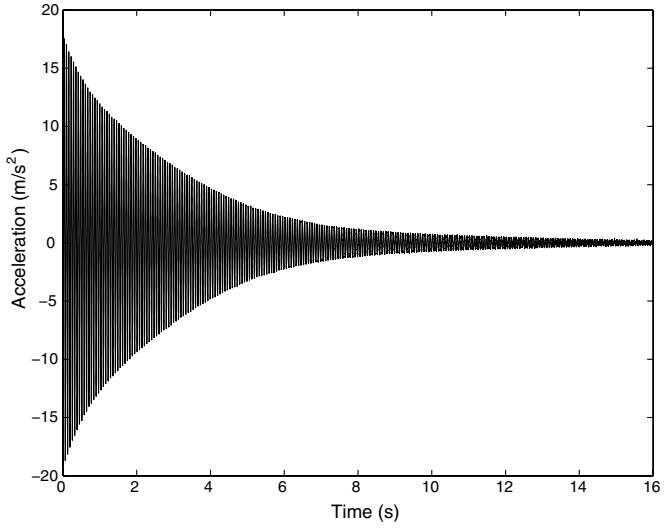

a) Response to hammer test

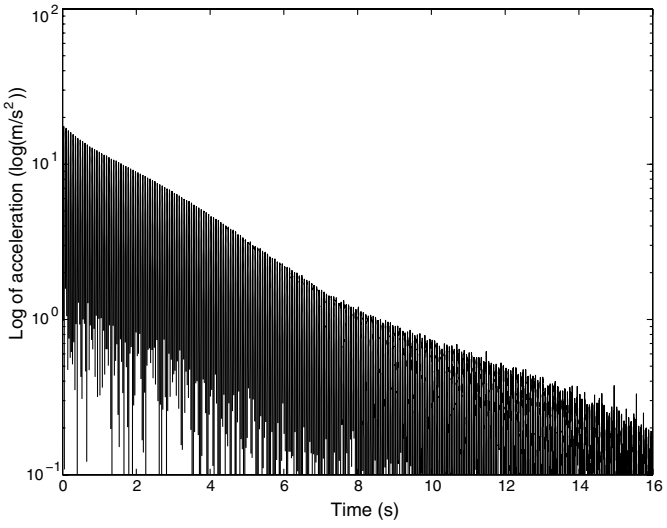

b) Log of response

Fig. 6 Acceleration response of store/pylon assembly 1 to hammer excitation.

To determine the nonlinearity present in the hammer-test results, the decaying response data were processed to yield the peak amplitudes per cycle to estimate the instantaneous damping and the period oscillation at each cycle to estimate the instantaneous frequency. The resulting instantaneous variations of natural frequency (actually damped natural frequency, but this is a small effect) for the two store/pylon assemblies are shown in Fig. 7; the frequency is seen to increase at higher amplitudes, as would be expected for a system featuring a hardening stiffness nonlinearity. The variation of instantaneous damping ratio against amplitude, determined from a series of different tests, is shown in Fig. 8; there is no obvious trend with amplitude, but the damping for store 1 is somewhat greater than that for store 2.

VI. Dynamic Characteristics of Wing/Store/Pylon

A. Modal Characteristics Random Excitation

Initial tests were performed on the model using two shakers with multiple uncorrelated burst random-excitation signals at several drive voltage levels. A sample FRF is shown in Figs. 9 and 10, zoomed into different frequency ranges. At the lower voltage levels, the FRFs were relatively unaffected by amplitude, but at the higher levels, the natural frequency increased and homogeneity was clearly not satisfied; this behavior is evidence of a hardening stiffness nonlinearity, as expected from the store/pylon static assembly tests. There is no obvious evidence from the FRFs of a change in damping with response amplitude. The equivalent results for modes 4 and 5 do not indicate any noticeable lack of homogeneity for the voltage levels applied.

The results from the random-excitation tests already provide several important pieces of information concerning the system:

1) The system contains nonlinearity that only significantly affects its response at relatively high levels of excitation.

2) The nonlinearity is of the hardening type, as it increases the natural frequencies seen in the FRFs.

3) The nonlinearity only affects the first three modes at the excitation levels considered. The other two modes with frequencies up to 135 Hz remain unaffected.

Consequently, a good nonlinear model of the structure under investigation in the range up to 150 Hz is expected to contain five modes, two of which are completely linear (modes 4 and 5) and three of which are nonlinear (modes 1, 2, and 3).

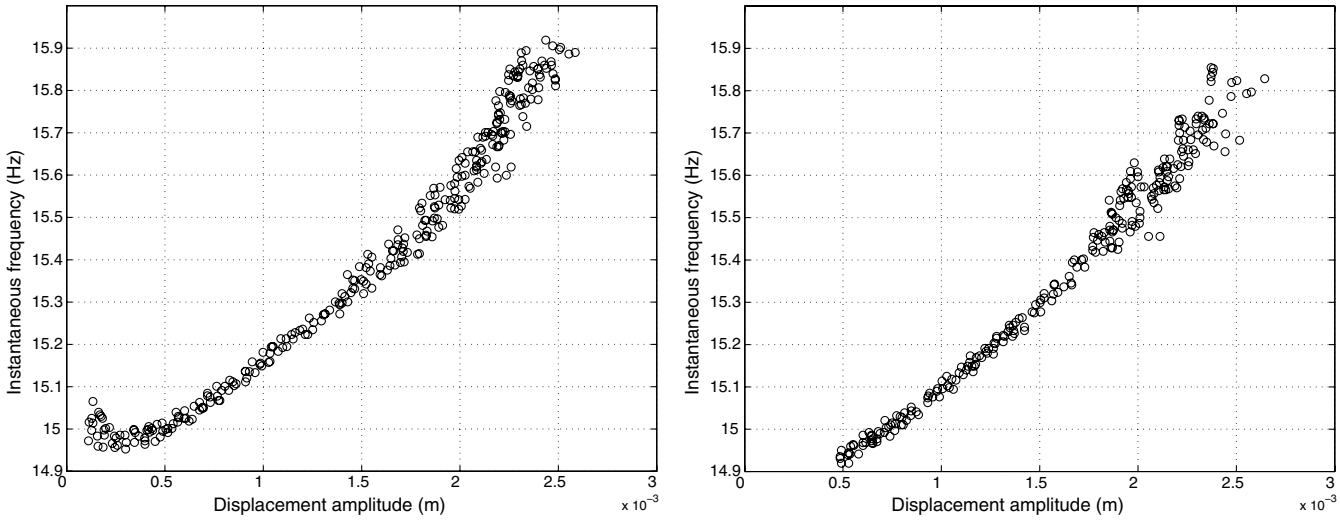

a) Store 1 b) Store 2

Fig. 7 Instantaneous response frequency against response amplitude for the two store/pylon assemblies.

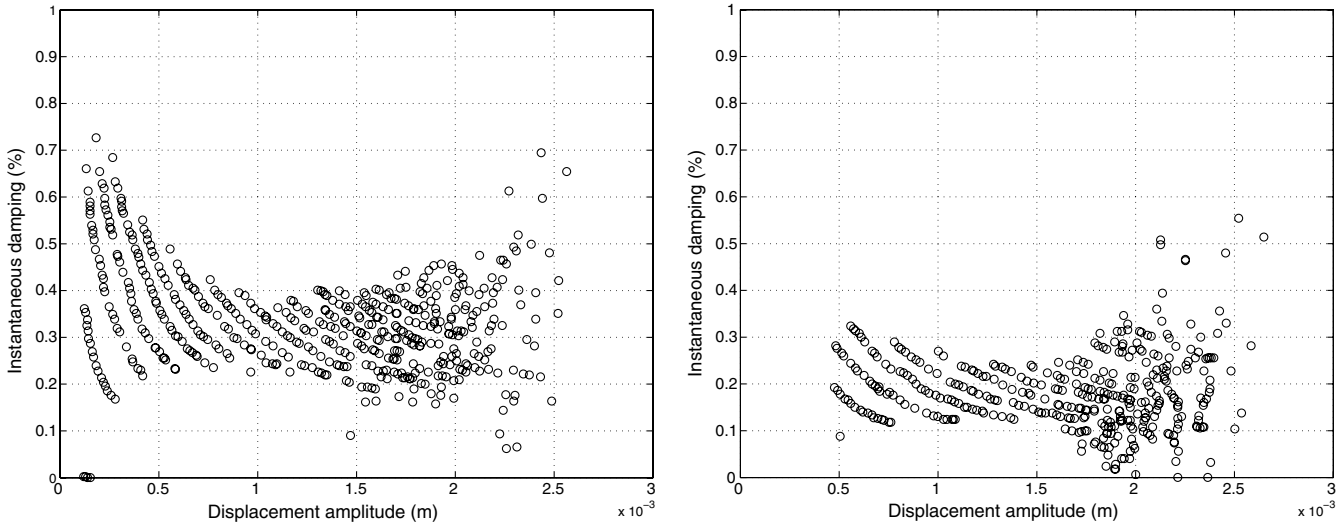

a) Store 1 b) Store 2

Fig. 8 Instantaneous response damping against response amplitude for the two store/pylon assemblies.

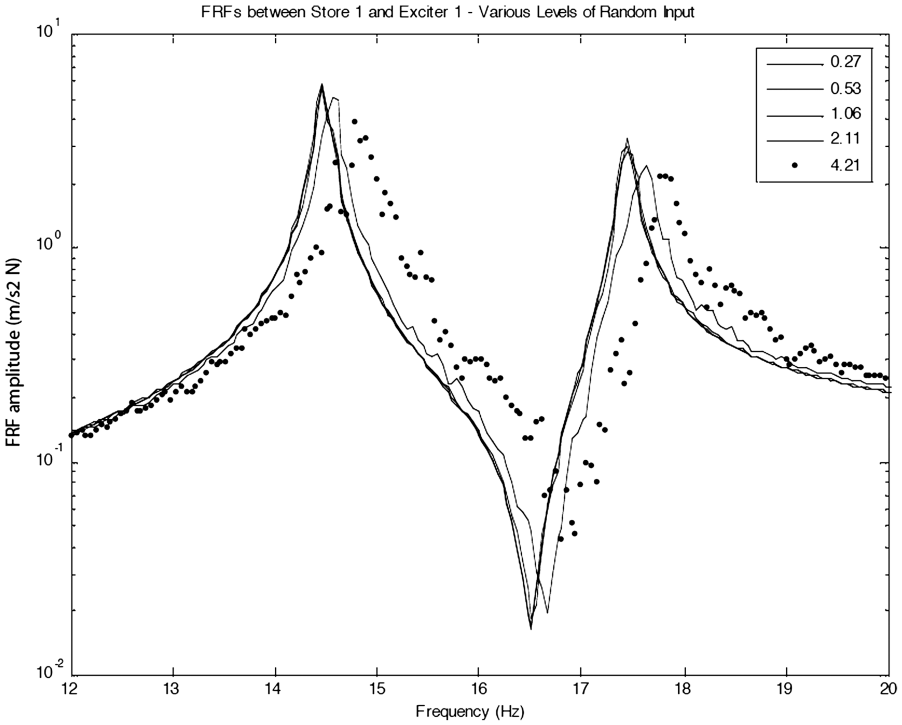

Fig. 9 FRFs between store 1 lateral and shaker 1 vertical around modes 1 and 2 for various levels of random input (volts).

The NL-RDM requires an estimate of the modal parameters of the underlying linear model. It was considered that the lower two levels in the random-excitation tests were sufficiently unchanged for the system's dynamic behavior in that excitation region to be treated as linear. The natural frequencies, damping ratios, and modal masses for the first five modes, extracted from the entire FRF matrix using the PolyMAX [21] parameter estimation method, are shown in Table 1.

The corresponding mode shapes are shown in Fig. 11. The modes shapes were found to be relatively independent of excitation level, as was also concluded by Göge et al. [16] from their practical experience on aerospace structures. Modes 1, 3, and 5 are symmetric and modes 2 and 4 are antisymmetric. Mode 2 is most sensitive to the differences in stiffness characteristics between the two pylons, displaying the greatest level of asymmetry. All the modes are nearly real, and so the damping is essentially proportional; nonproportional damping would have yielded linearly coupled modes. Modes 1 and 2 feature the highest levels of rotation between the store and the wing and are justifiably the most nonlinear. Mode 3 features a small degree of store rotation and is therefore less nonlinear than the first two modes. The amount of store rotation present in mode shapes 4 and 5 is negligible; these two modes are almost completely linear and will be treated as such throughout the rest of the present discussion.

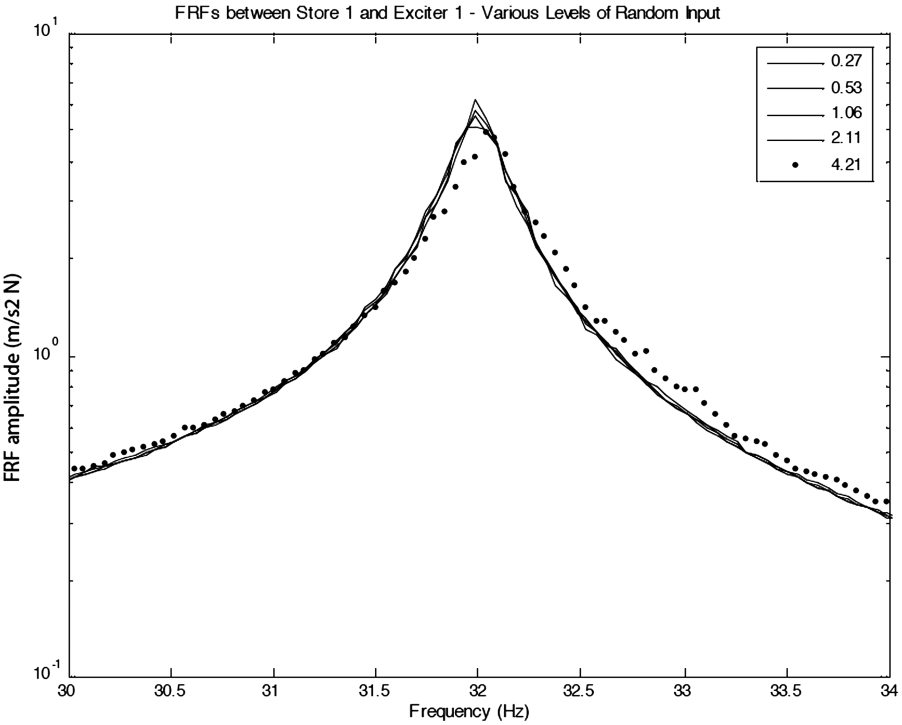

Fig. 10 FRFs between store 1 lateral and shaker 1 vertical around mode 3 for various levels of random input (volts).

Table 1 Natural frequencies, damping ratios, and modal masses estimated from low-level random-excitation tests

Mode	Natural frequency, Hz	Damping ratio, %	Modal mass, kg
1	14.45	0.50	2.00
2	17.42	0.49	2.36
3	31.96	0.61	1.51
4	76.47	0.33	0.94
5	131.80	0.31	1.03

Finally, the multivariate mode indicator function approach was applied to determine the force patterns required to excite each of the normal modes. The five modes occur when the MMIF drops to near zero. The appropriated force vectors are 1:0.95, 1: − 0.90, 1:1.10, 1: − 1.08, and 1:1.12. For modes 1, 3, and 5, the patterns reflect the symmetry, whereas for modes 2 and 4, the antisymmetry is evident.

B. Further Assessment of the Nonlinear Behavior of the System

To examine the nonlinear region beyond what was possible using random excitation, without risk of damaging the shaker, it was decided to apply a multiphase stepped sine approach with two shakers acting in or out of phase. In this approach, two force patterns are typically applied in turn (say, 1:1 and 1: − 1) at a range of frequencies; a steady-state response is sought at each frequency. The results are then combined to generate an FRF matrix. However, it was decided to examine only the response amplitude spectrum (not the FRF).

The pattern 1:1 was applied to excite mode 1 and the pattern 1: − 1 to excite mode 2, both at a range of excitation levels; any shaker/structure interaction was compensated for by use of a force amplitude/phase control. Amplitude spectra for modes 1 and 2 are shown in Fig. 12; it can be seen that the characteristic hardening stiffness behavior of a shift up in frequency followed by a jump down is evident in both modes. Mode 3 showed little nonlinearity for the force levels examined and so the results are not presented here.

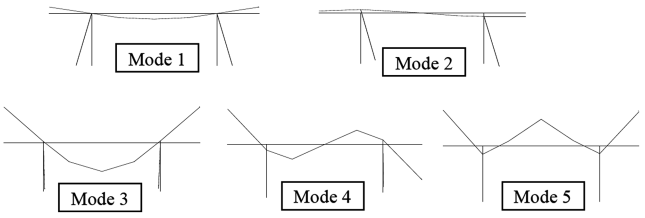

Fig. 11 First five mode shapes.

VII. Choice of Burst Excitation Signals for NL-RDM

The application of the NL-RDM requires a burst excitation of each mode, stopping sufficiently early that the response decays within the acquisition window so that leakage is minimized when any numerical integration of the measured acceleration signals is performed. Normally, the burst signal is a sine wave at the undamped natural frequency of interest and a triangular burst amplitude is employed, ramping up and down in amplitude to avoid severe transients (and so setting off responses in other modes, such as rigid-body motion).

The principle is that by applying a sine wave and increasing its amplitude, the system will respond sufficiently nonlinearly to allow a successful nonlinear identification. Also, by using an appropriated force pattern, the dominant excitation force will be applied to the mode of interest.

However, it was found for this wing/store/pylon structure that when seeking to excite either of the first two modes at their undamped natural frequencies, an inadequate level of response was obtained and that nonlinear features in the response data were not sufficiently prominent; by inspecting Fig. 12 it may be seen that this behavior is due to the fact that each undamped natural frequency (14.45 Hz for the first mode and 17.42 Hz for the second mode) was well below the frequency at which peak response occurred when employing stepped sine excitation. The figure shows that by working upward in frequency and using a stepped sine approach, it is possible to traverse the upper stable limb of the curve, thus generating a significantly higher amplitude than would be obtained at the natural frequency.

It was therefore decided to apply a burst narrowband chirp instead of a burst sine wave for modes 1 and 2. Here, the chirp excitation frequency started at a constant value and the excitation amplitude was ramped up. The frequency was then increased linearly, such that the modal response moved up the amplitude curve toward the maximum value at which the nonlinearity was being strongly exercised. The excitation was held at this end frequency and then ramped down, finally leaving time for the system to decay. The complete excitation signal was given by

$$f_r(t) = \begin{cases} \frac{A_0}{t_1} t \sin \omega_{r_1} t & \text{for } t < t_1 \\ A_0 \sin\left(\frac{\omega_{r_2}-\omega_{r_1}}{t_2-t_1}\left(\frac{t^2+t_1^2}{2} - t_1 t\right) + \omega_{r_1} t\right) & \text{for } t_1 < t < t_2 \\ A_0\left(1 - \frac{t-t_2}{t_f-t_2}\right) \sin(\omega_{r_2}(t-t_2) + \phi) & \text{for } t_2 < t < t_f \end{cases} \tag{13}$$

where

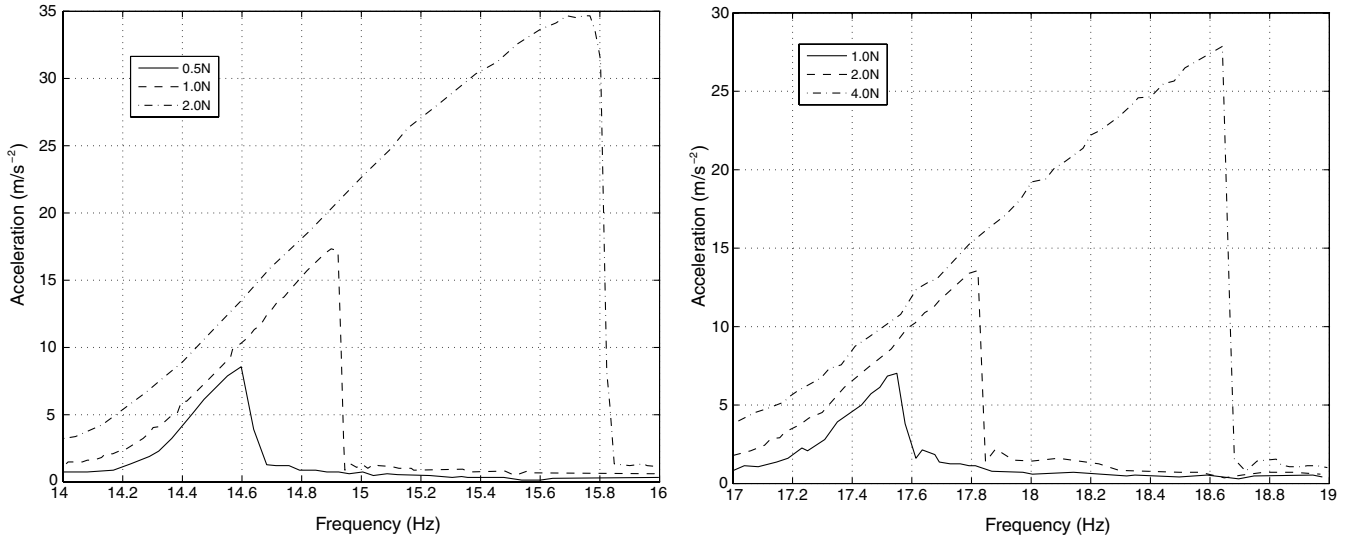

a) Mode 1 **b) Mode 2**

Fig. 12 Amplitude response to stepped sine excitation for modes 1 and 2.

$$\phi = \frac{\omega_{r_2} - \omega_{r_1}}{t_2 - t_1}\left(\frac{t_2^2 + t_1^2}{2} - t_1 t_2\right) + \omega_{r_1} t_2$$

and where ω_{r_1} and ω_{r_2} are frequencies lower and higher than the frequency of the mode of interest, respectively. Even though the excitation frequency is not held constant at the natural frequency, the force appropriation approach still works to an extent, as it acts as a coarse filter to minimize the response of the other modes (apart from those modes that are nonlinearly coupled to the mode being excited).

Mode 3 was tested using a standard burst sine wave of the form of Eq. (8), because it was not possible to drive the mode sufficiently strongly to achieve a significant frequency shift. Modes 4 and 5 were not identified using NL-RDM, because the linear modal parameters were assumed to be capable of fully describing them, as no apparent nonlinear behavior was evident in the FRFs generated from the random-excitation test results for these modes.

VIII. Identification of Nonlinear Characteristics Using NL-RDM

The NL-RDM was applied to the structure using two shakers with an appropriated excitation pattern for each mode of interest (i.e., modes 1 to 3). The physical forces and accelerations were measured; the modal forces and responses were then calculated by transforming the physical coordinate forces and responses to modal space using the modal matrix composed of the five mode shapes from the earlier linear identification at low excitation levels. For each mode, the modal accelerations were integrated in time to obtain modal velocities and displacements. These integrations were performed after a transformation to the frequency domain. The complete leakage-free signals were thus treated. The modal responses, modal kinetic energy, and modal power for each mode were examined and used to assist in deciding which direct and coupling terms to include in the nonlinear model for each mode.

Purely polynomial basis functions of order 3 were used for the construction of the nonlinear models, to keep the order of the model as low as possible. Equations (11) and (12) show that the nonlinearity in the store/pylon assemblies also contains quadratic terms. Therefore, a cubic-only curve fit is a simplification; however, it allows the construction of less complex nonlinear models that still represent the important dynamics of the system (i.e., hardening behavior). No nonlinear damping was modeled, as the random-excitation tests showed little evidence of such nonlinearity in the system.

The significance and parameter value of each term in the nonlinear model were determined by means of a nonlinear curve fit. The latter fit used data from only the steady-state and decaying parts of the response and excitation signals (i.e., from time $t = t_1$ to the time instance when all responses decayed to zero). The amplitude ramp-up sections of the data were neglected (i.e., from time $t = 0$ to t_1).

When performing nonlinear system identification it is necessary to use at least two data sets, one for the curve fit and one for validation, to ensure that the model fits the system and not just the data [1]. Half of the data points were selected at random to form the identification set, and the other half of the data points were used as a test set to determine the quality of the curve fit and to allow term selection.

The modal mass values used in the nonlinear curve fits were obtained from Table 1 (i.e., from the modal parameter estimation performed on the low-amplitude random-excitation data set). The linear damping and stiffness terms were calculated as part of the nonlinear curve-fitting process. Comparison with the linear PolyMAX results in Table 1 indicates a very good agreement for these terms. The complete nonlinear curve fit was therefore of the form

$$\begin{aligned} m_r \ddot{p}_r - f_r = &-c_r \dot{p}_r - k_r p_r - A_{1_r} p_1^3 - A_{2_r} p_1^2 p_2 - A_{3_r} p_1^2 p_3 \\ &- A_{4_r} p_1 p_2^2 - A_{5_r} p_1 p_2 p_3 - A_{6_r} p_1 p_3^2 - A_{7_r} p_2^3 - A_{8_r} p_2^2 p_3 \\ &- A_{9_r} p_2 p_3^2 - A_{10_r} p_3^3 \end{aligned} \tag{14}$$

for $r = 1, 2, 3$, where the unknowns to be evaluated were c_r, k_r, and A_{1_r} to A_{10_r}.

As the number of terms in this model is relatively small, the best model structure was chosen by performing an exhaustive search. Model structure selection is an essential part of nonlinear system identification procedures, because not every candidate term should be included in the final model. In other words, some of the A_{1_r} to A_{10_r} coefficients may have values of 0. Several structure selection procedures have been proposed in the literature, such as forward regression, backward elimination, orthogonal estimation [22], genetic algorithms [23], and others. All such procedures involve the evaluation of different models (i.e., different combinations of candidate terms). Each such combination is curve-fitted and assigned a quality-of-fit statistic. Finally, the model with the best quality of fit is selected.

An exhaustive search procedure implies that all the possible combinations of candidate terms are evaluated. The resulting model is the absolute optimum given particular sets of candidate terms and data. Such a procedure would be too computationally expensive for a large number of candidate terms but could be easily applied in the present case, due to the low number of candidate terms. Thus, one of the main advantages of the NL-RDM method is highlighted: by limiting the number of terms participating in the responses, the nonlinear models can be simpler and evaluated with more accuracy.

Figure 13 shows the variation of the quality-of-fit criterion against the number of nonlinear terms in the model. It must be stressed that the linear damping and stiffness terms were included by default; only nonlinear terms were subjected to the selection procedure. The quality-of-fit criterion used in this case was the mean square of the residual between measured and reconstructed responses: that is,

$$\text{MSE} = \frac{1}{N}\sum_{i=1}^{N}\left(\frac{p_r - \tilde{p}_r}{p_r}\right)^2$$

where MSE stands for mean square error, N is the number of measured time instances, p_r is the measured modal response, and $\tilde{p}_r$ is the modal response estimated from the time integration of the identified model. Figure 13 shows that five terms are enough to minimize the mean square of the residual for all three modes curve-fitted. However, it should be noted that the overall quality of fit for mode 2 is not as good as for mode 1, and that for mode 3 is the best. This suggests that the inclusion of second-order candidate terms might have been necessary in the curve fits of modes 1 and 2.

The final selected models and parameter estimates for all three modes are shown in Tables 2 and 3. Table 2 shows the estimates of the linear parameters (c_r and k_r) obtained from the nonlinear curve fits and compares them with those obtained from the PolyMAX modal estimation procedure. It can be seen that there are very small differences between the two sets of estimates, and this is encouraging.

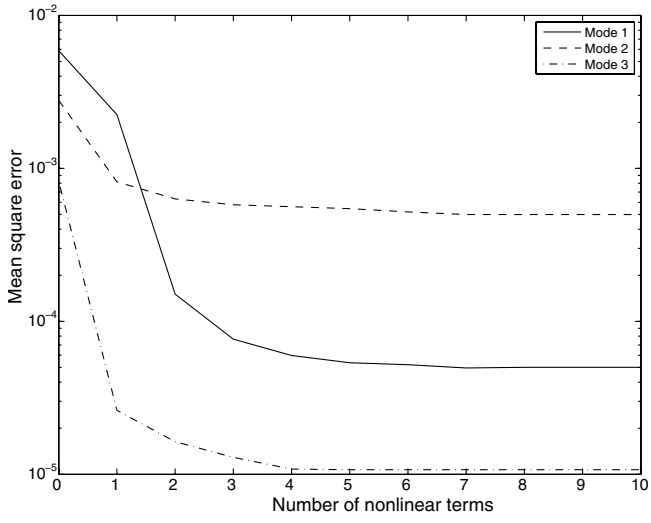

Fig. 13 Quality of fit against the number of nonlinear terms.

Table 2 Linear direct term coefficients for modes 1–3 identified by NL-RDM and PolyMAX

Mode	c_r NL-RDM	c_r PolyMAX	k_r NL-RDM	k_r PolyMAX
1	1.92	1.80	1.64×10^4	1.65×10^4
2	2.59	2.55	2.84×10^4	2.83×10^4
3	3.06	3.71	6.12×10^4	6.07×10^4

Table 3 shows the estimates for the nonlinear coefficients A_{1_r} to A_{10_r}. A zero value for one of these coefficients denotes that the corresponding term was not included in the final model.

Based on the parameter estimates presented in Tables 1–3 and the model structure of Eq. (14), the complete identified equations of motion for the wing/store/pylon system can be written as

$$
\begin{aligned}
&2.00\ddot{p}_1 + 1.92\dot{p}_1 + 1.64 \times 10^4 p_1 + 3.39 \times 10^8 p_1^3 - 1.53 \\
&\quad \times 10^9 p_1^2 p_2 - 7.70 \times 10^8 p_1^2 p_3 + 3.14 \times 10^9 p_1 p_2^2 - 9.49 \\
&\quad \times 10^7 p_3^3 = f_1(t) \\
&2.36\ddot{p}_2 + 2.59\dot{p}_2 + 2.84 \times 10^4 p_2 + 5.93 \times 10^9 p_1^2 p_2 - 1.32 \\
&\quad \times 10^{10} p_1 p_2 p_3 + 1.13 \times 10^9 p_2^3 + 1.65 \times 10^9 p_2^2 p_3 + 2.15 \\
&\quad \times 10^{10} p_2 p_3^2 = f_2(t) \\
&1.51\ddot{p}_3 + 3.06\dot{p}_3 + 6.12 \times 10^4 p_3 - 2.34 \times 10^8 p_1^3 + 1.47 \\
&\quad \times 10^9 p_1^2 p_3 + 6.42 \times 10^{10} p_1 p_2 p_3 - 2.31 \times 10^9 p_1 p_3^2 + 1.34 \\
&\quad \times 10^9 p_2 p_3^2 = f_3(t) \\
&0.94\ddot{p}_4 + 2.92\dot{p}_4 + 2.16 \times 10^5 p_4 = f_4(t) \\
&1.03\ddot{p}_5 + 5.28\dot{p}_5 + 7.03 \times 10^5 p_5 = f_5(t)
\end{aligned} \tag{15}
$$

It should be mentioned that under appropriated excitation, the amplitudes of the cross-coupled modal responses were about an order of magnitude lower than those of the direct modal responses. Therefore, all the cross-coupled nonlinear terms in Eqs. (15) are at least an order of magnitude smaller than the direct nonlinear terms. This difference demonstrates that the purpose of the cross-coupling terms in the nonlinear curve fit is mainly to improve the accuracy of the identification of the direct terms.

A. Identification of Mode 1

For the symmetric mode 1, involving considerable store motion, the fit yielded cubic hardening direct terms involving modes 1 and 3 but also some cross-coupling terms between modes 1,2 and 1,3. The terms involving mode 2 suggest either some lack of symmetry in mode 1 or an imperfect appropriation. The measured and curve-fitted restoring force surfaces for this mode are compared in three dimensions in Fig. 14a. The two-dimensional section of these surfaces for $\dot{p}_1 = 0$ is plotted in Fig. 14b. Both figures show that the quality of the identification of the restoring force surface is very good. The presence of hardening stiffness nonlinearity for this mode is very clear.

Table 3 Nonlinear term coefficients identified for modes 1–3

Coefficient	Mode 1	Mode 2	Mode 3
A_{1_r}	3.39×10^8	0	-2.34×10^8
A_{2_r}	-1.53×10^9	5.93×10^9	0
A_{3_r}	-7.70×10^8	0	1.47×10^9
A_{4_r}	3.14×10^9	0	0
A_{5_r}	0	-1.32×10^{10}	6.42×10^{10}
A_{6_r}	0	0	-2.31×10^9
A_{7_r}	0	1.13×10^9	0
A_{8_r}	0	1.65×10^9	0
A_{9_r}	0	2.15×10^{10}	1.34×10^9
A_{10_r}	-9.49×10^7	0	0

B. Identification of Mode 2

Here, a similar approach was used as for mode 1, except that a different force pattern and frequency range were obviously employed. In this case, a cubic hardening term in mode 2 was identified, along with coupling terms involving all three modes. The measured and curve-fitted modal restoring force surfaces are shown in Fig. 15, again in 3-D and 2-D views. The presence of a hardening stiffness nonlinearity for this mode is also very clear and the agreement between the measured and fitted surfaces is very good.

C. Identification of Mode 3

For this mode, a burst sine appropriated force was applied, as mentioned previously. The identification yielded a direct cubic term in mode 1 and several cross-coupling terms involving all three modes. However, the direct cubic term in mode 3 is noticeable by its absence. It is believed that this absence is due to the fact that the behavior of mode 3 was only mildly nonlinear, as seen from the random-excitation test results. As usual, the measured and fitted modal restoring force surfaces are shown in Fig. 16 in 3-D and 2-D views. The presence of a hardening stiffness nonlinearity for this mode is not apparent in these plots. In fact, the 2-D section of Fig. 16b

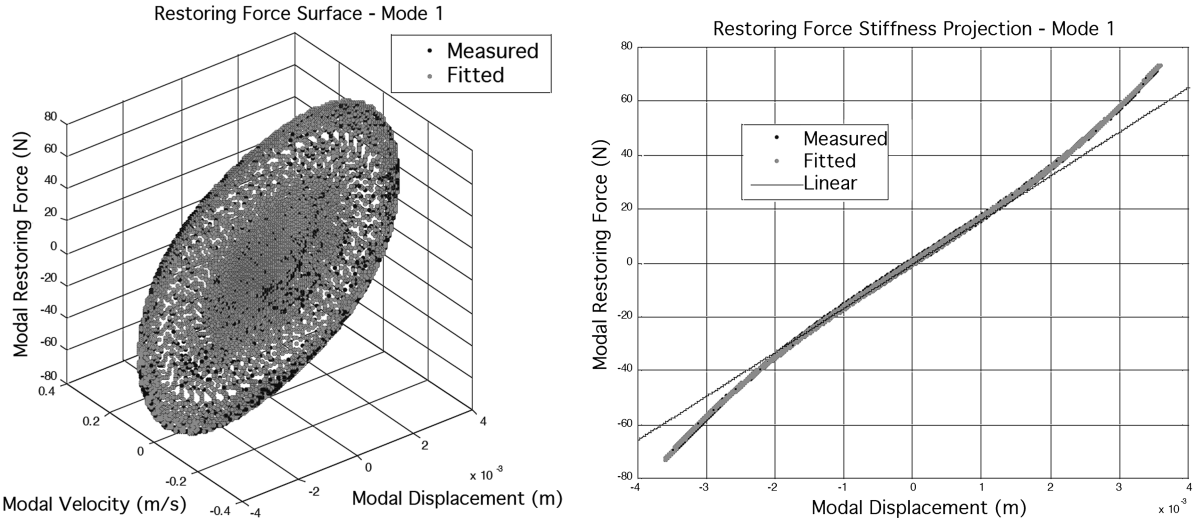

a) 3-D surface b) 2-D section

Fig. 14 Comparison of mode 1 measured and curve-fitted restoring force surface.

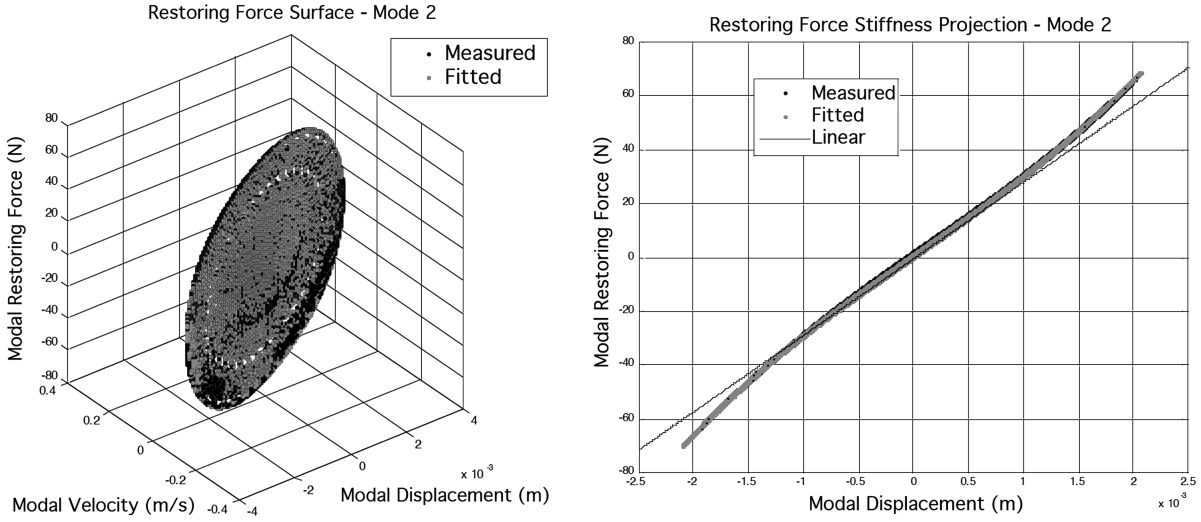

a) 3-D surface **b) 2-D section**

Fig. 15 Comparison of mode 2 measured and curve-fitted restoring force surface.

appears almost linear. Nevertheless, the agreement between the measured and fitted restoring force surfaces is good.

It is possible that higher-amplitude excitation might have yielded more obviously nonlinear responses. However, it was found practically impossible to excite this mode at a higher level without endangering the experimental model and instrumentation.

D. Rigid-Body Modes

The wing/store/pylon structure was suspended upon bungees from a frame. As such, the arrangement of the instrumentation and shakers allowed rigid-body motion in heave (vertical displacement), roll (rotation around the wing's centerline), and sway (in-plane displacement in the spanwise direction). It was assumed that the bungees behaved linearly and, therefore, the rigid-body modes did not couple nonlinearly to the elastic modes. It can often be difficult to identify the rigid-body mode characteristics experimentally when the frequencies are very low, because of imperfect shaker and accelerometer performance at such frequencies.

XI. Model Validity

In all system identification, the final mathematical model reflects only the aspects of the original system that were tested and used in the identification process. Any features of the system that were not measured and/or not curve-fitted will not be reflected by the model. Therefore, the range of validity of a model is limited by the test conditions. Outside the range of validity, linear identified models are no longer representative of the system. However, when nonlinear identified models are used outside the range of validity, they may well fail completely (i.e., they can be unstable), especially when the model contains polynomial terms.

As explained earlier, the NL-RDM uses appropriated excitation to generate the force and response data that will be used in the nonlinear curve fit. This means that for each mode to be identified, the response data contain major contributions from this same mode and minor contributions from other, nonlinearly coupled, modes. Therefore, the nonlinear terms depending only on the mode under consideration will be identified with a large range of validity, corresponding to the maximum excitation amplitude applied to this mode, whereas the cross terms will have a much smaller range of validity, because the other modes are not excited to the same extent. It follows that any nonlinear model obtained from appropriated excitation data will not be representative of the true system in the case in which all modes may be excited to a large extent. And, as polynomial curve fits very often blow up when extrapolated, it is logical that identified models of this type may become unstable when they are used under nonrepresentative conditions.

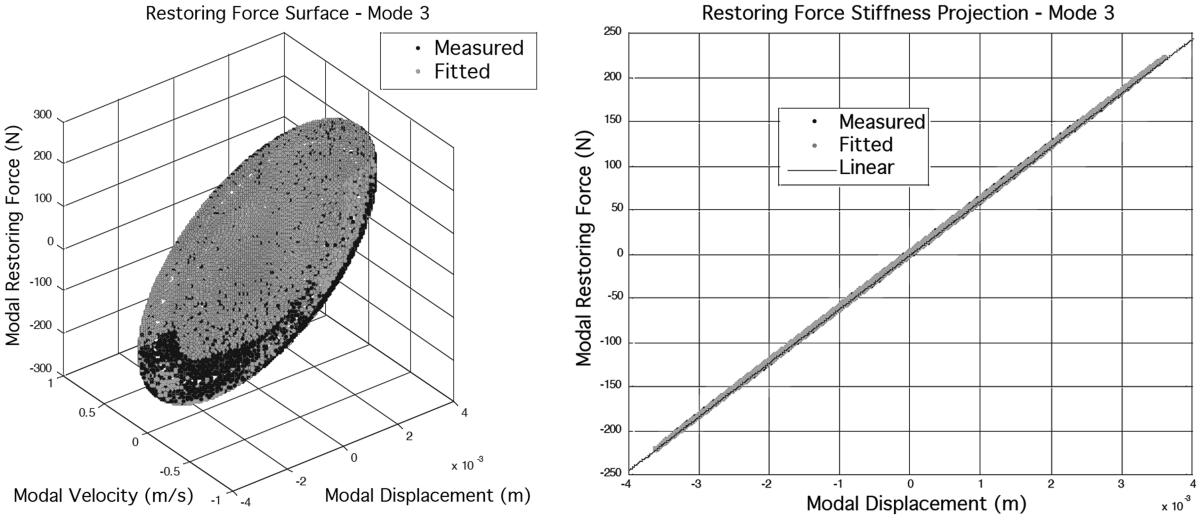

a) 3-D surface **b) 2-D section**

Fig. 16 Comparison of mode 3 measured and curve-fitted restoring force surface.

Figures 14–16 show that the data measured from the system featured modal displacements of amplitude ±4 mm in all three modes. Therefore, the identified model should be representative up to this response amplitude. The amplitude of the modal velocities is not critical, because no nonlinear damping terms were included in the model. The identified model of Eqs. (15) is valid for the case in which only one of the nonlinear modes (p_1, p_2, or p_3) responds with an amplitude in the ±4 mm range; the other two modes must be excited to a much smaller amplitude range for the model to be valid.

When all three modes respond at high amplitudes, Eqs. (15) become unstable because the nonlinear coupling terms are extrapolated. In this case, the nonlinear submodel including only direct terms can be used: that is,

$$
\begin{aligned}
&2.00\ddot{p}_1 + 1.92\dot{p}_1 + 1.64 \times 10^4 p_1 + 3.39 \times 10^8 p_1^3 = f_1(t)\\
&2.36\ddot{p}_2 + 2.59\dot{p}_2 + 2.84 \times 10^4 p_2 + 1.13 \times 10^9 p_2^3 = f_2(t)\\
&1.51\ddot{p}_3 + 3.06\dot{p}_3 + 6.12 \times 10^4 p_3 = f_3(t)\\
&0.94\ddot{p}_4 + 2.92\dot{p}_4 + 2.16 \times 10^5 p_4 = f_4(t)\\
&1.03\ddot{p}_5 + 5.28\dot{p}_5 + 7.03 \times 10^5 p_5 = f_5(t)
\end{aligned}
\tag{16}
$$

It can be seen that there are only two nonlinear modes now, modes 1 and 2, as the nonlinear terms in mode 3 were all indirect or cross-coupling terms (i.e., there was no nonlinear term involving only p_3). Mode 3 is now an uncoupled linear term, just like modes 4 and 5. It must be stressed that despite the fact that the Eq. (16) only contains direct nonlinear terms, it is more accurate than the equation that would have been identified if only direct terms had been considered in the curve fit. In this latter case, the coefficients of the direct nonlinear terms would contain contributions from the cross-coupling terms. This inaccuracy is not present in the identified model of Eq. (16).

X. Conclusions

In this paper, an aircraftlike nonlinear continuous wing/store/pylon experimental structure was identified using the NL-RDM approach. Discrete hardening stiffness nonlinearity was located in the pylon rotation degrees of freedom. The results showed evidence of a hardening nonlinear stiffness at higher amplitudes for the first three modes. The NL-RDM succeeded in estimating good-quality nonlinear modal models for the first three modes, with direct hardening nonlinearity terms in modes 1 and 2. Mode 3, although nonlinearly coupled to the first two modes, did not feature direct hardening stiffness itself. Modes 4 and 5 behaved linearly and so a linear modal model sufficed.

The paper describes a complete successful application of the NL-RDM methodology, starting with a first characterization of the system and ending with a full five-mode combined linear and nonlinear mathematical model that corresponded very well with the measured data. Several particularities of the system are highlighted and the necessary adaptations of the NL-RDM are described. The validity of the resulting identified model is explored and the advantages of force appropriation-based nonlinear system identification are discussed. In the future, the NL-RDM technique will be applied to other test data featuring different nonlinearities.

Acknowledgments

The Engineering and Physical Sciences Research Council (EPSRC) of the United Kingdom funded this research. The authors acknowledge the assistance of K. Worden, University of Sheffield.

References

[1] Worden, K., and Tomlinson, G. R., *Nonlinear Vibrations*, Sheffield Univ. Press, Sheffield, England, U.K., 2000.

[2] Fargette, P., Füllekrug, U., Gloth, G., Levadoux, B., Lubrina, P., Schaak, H., and Sinapius, M., "Tasks for Improvement in Ground Vibration Testing of Large Aircraft," *CEAS/AIAA International Forum on Aeroelasticity and Structural Dynamics (IFASD 2001)*, Vol. 3, Asociación de Ingenieros Aeronáuticos, España, Spain, June 2001, pp. 121–133.

[3] Wright, J. R., Platten, M. F., Cooper, J. E., and Sarmast, M., "Identification of Multi Degree of Freedom Weakly Nonlinear Systems Using a Model Based in Modal Space," *Proceedings of the COST International Conference on Structural System Identification* [CD-ROM], Universitätsbibliothek Kassel, Kassel, Germany, 2001, pp. 49–68.

[4] Platten, M. F., Wright, J. R., Dimitriadis, G., and Cooper, J. E., "Identification of Multidegree of Freedom Nonlinear Systems Using an Extended Modal Space Model," *Mechanical Systems and Signal Processing*, Vol. 23, No. 1, 2009, pp. 8–29. doi:10.1016/j.ymssp.2007.11.016

[5] Gloth, G., and Sinapius, M., "Influence and Characterisation of Weak Nonlinearities in Swept-Sine Modal Testing," *Aerospace Science and Technology*, Vol. 8, No. 2, 2004, pp. 111–120. doi:10.1016/j.ast.2003.09.005

[6] Lind, R., Snyder, K., and Brenner, M., "Wavelet Analysis to Characterise Non-Linearities and Predict Limit Cycles of an Aeroelastic System," *Mechanical Systems and Signal Processing*, Vol. 15, No. 2, 2001, pp. 337–356. doi:10.1006/mssp.2000.1346

[7] Benini, G., Cooper, J., and Wright, J. R., "Quantification of Aircraft Non-Linearities from Flight Flutter Test Data," *International Conference on Noise and Vibration Engineering (ISMA 2004)* [CD-ROM], Katholieke Univ. Leuven, Leuven, Belgium, Sept. 2004, pp. 2079–2090.

[8] Göge, D., Sinapius, M., Füllekrug, U., and Link, M., "Detection and Description of Non-Linear Phenomena in Experimental Modal Analysis Via Linearity Plots," *International Journal of Non-Linear Mechanics*, Vol. 40, No. 1, 2005, pp. 27–48. doi:10.1016/j.ijnonlinmec.2004.05.011

[9] Göge, D., "Fast Identification and Characterization of Nonlinearities in Experimental Modal Analysis of Large Aircraft," *Journal of Aircraft*, Vol. 44, No. 2, 2007, pp. 399–409. doi:10.2514/1.20847

[10] Göge, D., Füllekrug, U., Sinapius, M., Link, M., and Gaul, L., "Advanced Test Strategy for Identification and Characterization of Nonlinearities of Aerospace Structures," *AIAA Journal*, Vol. 43, No. 5, 2005, pp. 974–986. doi:10.2514/1.5651

[11] Hu, Z., and Blakrishnan, S. N., "Parameter Estimation in Nonlinear Systems Using Hopfield Neural Networks," *Journal of Aircraft*, Vol. 42, No. 1, 2005, pp. 41–53. doi:10.2514/1.3210

[12] Dimitriadis, G., Vio, G. A., and Cooper, J. E., "Identification of Non-Linear Dynamic Systems Using an Expert Approach," 47th AIAA/ASME/ASCE/AHS/ASC Structures, Structural Dynamics and Materials Conference, Newport, RI, AIAA Paper 2006-2037, May 2006.

[13] Platten, M. F., Wright, J. R., and Cooper, J. E., "The Use of a Noncontact Acoustic Excitation Array for the Estimation of Damping in Aircraft Panels," *Proceedings of the 25th International Seminar on Modal Analysis (ISMA 2002)* [CD-ROM], Katholieke Univ. Leuven, Leuven, Belgium, Sept. 2002, pp. 451–460.

[14] Masri, S. F., Sassi, H., and Caughey, T. K., "Nonparametric Identification of Nearly Arbitrary Nonlinear Systems," *Journal of Applied Mechanics*, Vol. 49, No. 3, 1982, pp. 619–628.

[15] Williams, R., Crowley, J., and Vold, H., "The Multivariate Mode Indicator Function in Modal Analysis," *Proceedings of the 3rd International Modal Analysis Conference*, Society for Experimental Mechanics, Bethel, CT, 1985, pp. 66–70.

[16] Göge, U., Füllekrug, M., Sinapius, M., Link, M., and Gaul, L., "INTL a Strategy for the Identification and Characterization of Nonlinearities Within Modal Survey Testing," *Proceedings of the 22nd International Modal Analysis Conference (IMAC XXII)*, Society for Experimental Mechanics, Bethel, CT, 2004.

[17] Atkins, P. A., Wright, J. R., and Worden, K., "An Extension of Force Appropriation to the Identification of Non-Linear Multi-Degree of Freedom Systems," *Journal of Sound and Vibration*, Vol. 237, No. 1, 2000, pp. 23–43. doi:10.1006/jsvi.2000.3033

[18] Yang, Z., Dimitriadis, G., Vio, G. A., Cooper, J. E., and Wright, J. R., "Identification of Structural Free-Play Nonlinearities Using the Non-Linear Resonant Decay Method," *Proceedings of the International Conference on Noise and Vibration Engineering, ISMA 2006* [CD-ROM], Katholieke Univ. Leuven, Leuven, Belgium, 2006, pp. 2797–2810.

[19] Breitbach, E., "Effects of Structural Nonlinearities on Aircraft Vibration and Testing," AGARD Rept. R-665, Neuilly-sur-Seine, France, Jan. 1978.

[20] Beran, P. S., Strganac, T. W., Kim, K., and Nichkawde, C., "Studies of Store-Induced Limit-Cycle Oscillations Using a Model with Full System Nonlinearities," *Nonlinear Dynamics*, Vol. 37, No. 4, 2004, pp. 323–339. doi:10.1023/B:NODY.0000045544.96418.bf

[21] Peeters, B., Van der Auweraer, H., Guillaume, P., and Leuridan, J., "The PolyMAX Frequency-Domain Method: A New Standard for Modal Parameter Estimation?" *Shock and Vibration*, Vol. 11, Nos. 3–4, 2004, pp. 395–409.

[22] Billings, S., Chen, S., and Korenberg, M., "Identification of MIMO Nonlinear Systems Using a Forward Regression Orthogonal Estimator," *International Journal of Control*, Vol. 49, No. 6, 1989, pp. 2157–2189. doi:10.1080/00207178908559767

[23] Chen, Q., Worden, K., Peng, P., and Leung, A., "Genetic Algorithm with an Improved Fitness Function for (N)ARX Modelling," *Mechanical Systems and Signal Processing*, Vol. 21, No. 2, 2007, pp. 994–1007. doi:10.1016/j.ymssp.2006.01.011